



# Performance of the Deeply Embedded Ring Anchor under vertical loading in drained sand

R. Gogoi\*

*Triton Anchors, New York, USA*

A. Aldawwas

*Qassim University, Buraydah, KSA*

C. Aubeny

*Texas A&M University, College Station, USA*

D. DeGroot, S. Arwade

*University of Massachusetts Amherst, Amherst, USA*

A. Martinez

*University of California Davis, Davis, USA*

R. Beemer

*Virginia Tech, Blacksburg, USA*

\*[raginigogoi@tamu.edu](mailto:raginigogoi@tamu.edu) (corresponding author)

**ABSTRACT:** The presented study introduces a framework for evaluating the vertical capacity of the Deeply Embedded Ring Anchor (DERA) in sand, focusing on key parameters such as embedment depth and soil density. Previous research has predominantly examined DERA's performance in clay, but there is limited understanding of its behaviour in sand. To address this gap, finite element simulations were conducted, modeling the anchor's response to vertical monotonic loads, as a first stage study. The analysis investigates the effects of embedment depth on failure mechanisms, transitioning from surface failure at shallow depths to localized flow around failure at greater depths. The study also explores the influence of relative soil density on anchor performance. The parametric test series was used to develop a predictive model for estimating the ultimate vertical capacity of DERA as a function of relative density and embedment depth. The results demonstrate DERA's high anchor efficiency and contribute to the optimization of its design for floating offshore wind turbine foundations.

**Keywords:** Offshore Geotechnics, floating wind farm anchor, sand, vertical capacity.

## 1 INTRODUCTION

The Deeply Embedded Ring Anchor (DERA) (previously known as the Multiline Ring Anchor, MRA) is a novel anchor system developed to address the growing need for efficient anchoring solutions in offshore renewable energy, particularly for floating wind turbines (USA Patent No. US 2020/0407021 A1, 2019). DERA features a hollow cylindrical design with a thin wall (Figure 1), enabling deep embedment into the seabed, thereby enhancing geotechnical efficiency by utilizing deeper soil resistances while minimizing the impact of surface disturbance. This design allows for smaller anchors to meet the growing anchor demands of the market. Preliminary studies have demonstrated the supply chain benefits resulting from the simplicity of the anchor's geometry, in terms of required port and manufacturing facilities (Lee, Khan, Bello, & Aubeny, 2020). These advantages

make the anchor a potential alternative to available anchoring systems in the market, with the ability to reduce costs related to fabrication, transportation, and installation. The anchor also offers unique versatility, supporting installation in various soil types, including sand and stiff clay, and facilitates multiple mooring configurations—catenary, taut, and semi-taut. Such adaptabilities make DERA a strong contender for networked offshore wind farms, where the system geometry makes anchor sharing feasible.

As part of a broader proof-of-concept study, this paper proposes a framework for evaluating the vertical capacity of DERA in sand, as a function of its embedment depth and the soil density. While previous publications have investigated the anchor's performance in clay, (Aubeny & Lee, 2021) (Lee & Aubeny, 2021)—demonstrating promising capacity under various loading conditions—there has been

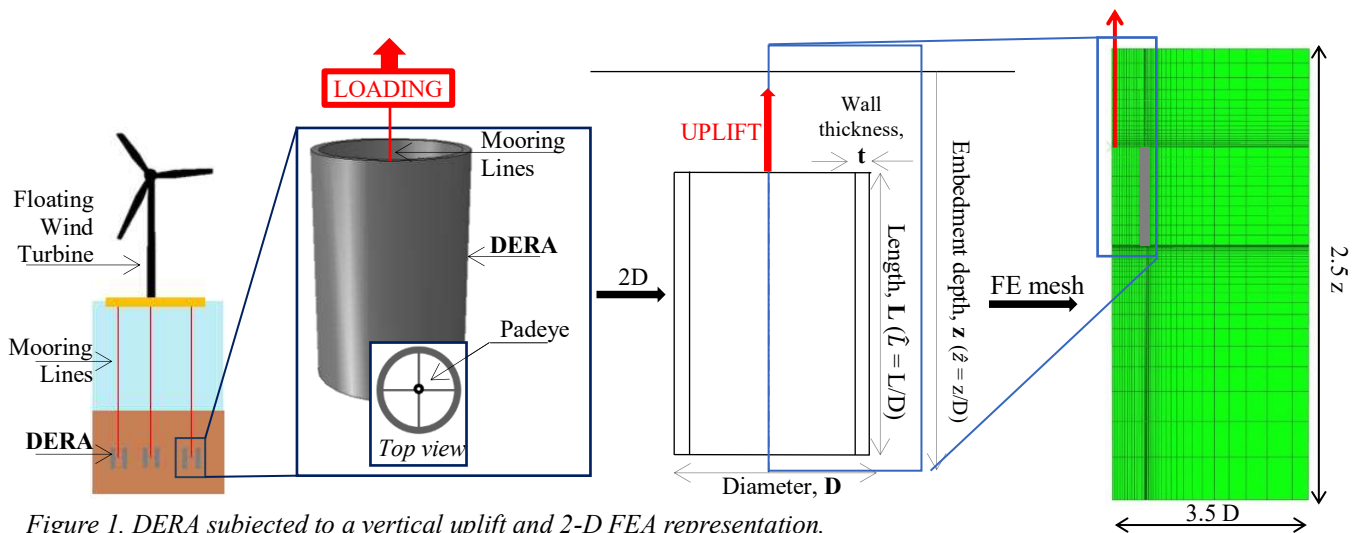


Figure 1. DERA subjected to a vertical uplift and 2-D FEA representation.

minimal research on its behavior in sandy sediments (Gogoi R., et al., 2023), (Aldawwas, 2022). This paper addresses that gap by studying the anchor's response to vertical monotonic loads in fully drained sand. The proposed framework analyzes key parameters, such as embedment depth and soil density, and examines their influence on the underlying mechanisms governing the anchor's overall performance. The insights gained from this study deepen the understanding of DERA's monotonic behavior in drained sand, laying the foundation for future investigations into more complex loading conditions.

## 2 NUMERICAL MODEL

### 2.1 Finite element model

The numerical analysis conducted for the study utilized the finite element formulation in ABAQUS/Standard/6.12.1. The objective of the model was to simulate the behavior of DERA subjected to a monotonic pure uplift, in fully drained sand. The inherent symmetry of the anchor and the loading condition allowed for the implementation of a two-dimensional, axisymmetric model. A displacement control analysis was performed, where the anchor was subjected to a uniform loading until the failure threshold was reached, set equal to a displacement magnitude of 10% of the anchor diameter.

The model comprised of a rigid, wished-in-place anchor in an isotropic soil with a stress dependent Young's Modulus,  $E$ . The soil domain and the anchor were modeled using four-node solid continuum displacement elements (CAX4) from the ABAQUS element library, with nodal boundary conditions applied along the far field and bottom edge of the mesh to constraint their vertical and/or horizontal movement

(Figure 1). The domain size was set at 2.5 times the anchor's vertical embedment depth and to the greater of either three times the diameter or one-third of the domain's vertical length radially. The selected dimensions accounted for the extent of the anchor's interaction with the surrounding soil as well as mitigate the potential influence of the prescribed boundary conditions on the analysis.

The soil-structure interaction along the walls of the anchor were described using the Coulomb friction model, with the coefficient of friction defined as a function of the interface friction angle. In the software, a node-to-surface contact discretization was selected with a small-sliding approach and default built-in model parameters to simulate the sliding behavior. At the tip interfaces, the action of the axial pull causes the anchor to exert an upward normal force against the soil at its top tip, potentially creating regions of high stress concentrations, while at the bottom tip, the stresses reduce to zero (AlHakeem & Aubeny, 2019), allowing the anchor to break away from the soil. To prevent potential mesh instability caused by the gap formation, this region was remodeled using low-stiffness elastic elements, engineered to mirror the field response by expanding vertically with the anchor upon loading (Gogoi, Aubeny, Watson, & Bransby, 2021). The accuracy of this modification is demonstrated in Figure 2, with the modified case exhibiting an additional advantage of a more favorable run time.

### 2.2 Material parameters

The soil failure mechanism in the numerical model was defined using an elastoplastic Mohr Coulomb constitutive model with a non-associative flow rule. The model parameters were defined as functions of the mean effective soil stress and the relative density. The Young's Modulus,  $E$ , was defined in terms of the rigidity index as (Vesic A. S., 1972) follows:

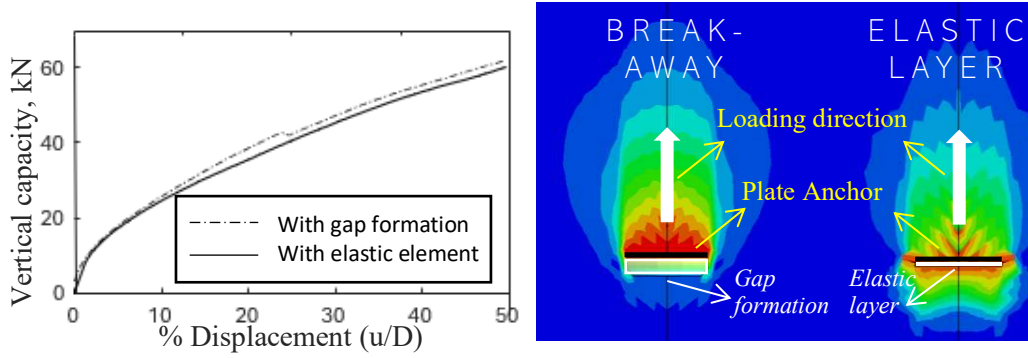


Figure 2. FE response of plate anchor under a vertical load, with formation of a gap vs. an elastic layer.

$$E = I_r(2(1 + \nu)(\sigma_v' \tan \varphi_{max})) \quad (1)$$

where  $E$  is a function of a density and stress-level dependent rigidity index,  $I_r$ , as proposed by Al Hakeem (AlHakeem & Aubeny, 2019). The strength parameters of the model, the angle of internal friction and the corresponding dilation angle were defined using the Bolton equations (Bolton M. , 1986) as follows:

$$0.8\psi_{max} = 3I_R = \varphi_{max} - \varphi_{crit} \quad (2)$$

$$I_R = I_D(10 - \ln \sigma_{mean}') - 1 \quad (3)$$

where  $\varphi_{max}$  is the peak friction angle,  $\varphi_{crit}$  is the critical state angle,  $\psi_{max}$  is the dilation angle,  $I_R$  is the relative dilatancy index, defined using the relative density of the soil,  $I_D$  and mean effective stress,  $\sigma_{mean}'$ .

The study focused on Ottawa F-65 sand with a saturated unit weight of  $20.18 \text{ kN/m}^3$ , Poisson's ratio,  $\nu$ , of 0.3 and critical friction angle,  $\varphi_{crit}$ , of  $30^\circ$  (Bastidas, 2016). Also, a geostatic step was introduced in the FEA model to simulate the initial stress conditions. The anchor is modeled as an aluminum structure of 70 GPa Young's Modulus, and Poisson's ratio of 0.3.

### 2.3 Calibration of numerical model

To certify the credibility of the predictions generated by the established numerical model, it was calibrated using data from reduced-scale centrifuge tests conducted in parallel at the Center for Geotechnical Modeling (CGM) at the University of California, Davis (Huang, et al., 2024). The physical tests were performed in a 9-meter radius centrifuge at 70-g for two anchor embedment depths ( $\hat{z}$  ( $z/D$ ) = 3 and  $\hat{z}$  ( $z/D$ ) = 6) in medium-dense to dense sand. The prototype model was pushed into the soil quasi-statically at 1-g, which was replicated in the numerical

model by introducing a column of reduced density soil in the installation path. The modification contributed to the successful calibration of the numerical model, with error percentages  $\leq \sim 5\%$ , as described in (Gogoi R. , 2024), and (Gogoi R. , et al., 2023), along with additional details of the developed finite element model. The resulting load-displacement response of the model with the measured data is presented in Figure 3, where the predictions demonstrate a stiffer initial response, but achieves capacity (defined at a failure threshold of 10% D) within acceptable limits.

### 3 EFFECT OF EMBEDMENT DEPTH

To study the effects of the anchor embedment depth on its capacity, a 2.8 m diameter ( $D$ ) anchor with a wall thickness of  $t = D/160$  and aspect ratio of  $L/D = 1.5$  at different embedment depths was analyzed using the finite element model. The results of the simulations are presented in Figure 4 in the form of load – normalized embedment depth,  $\hat{z}$  ( $z/D$ ), plots decomposed into base resistance and friction resistance components.

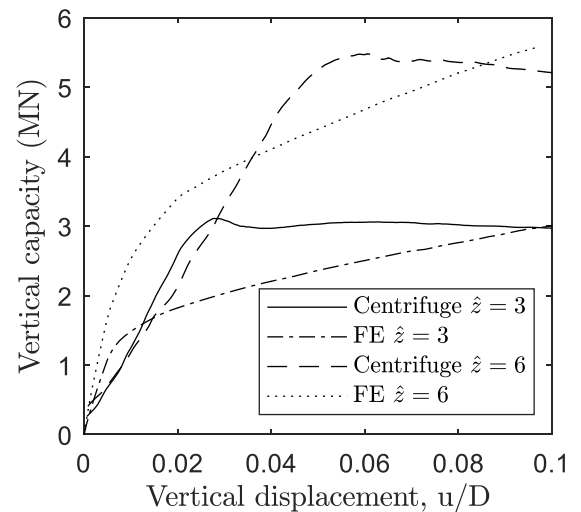


Figure 3. Load-displacement curves from centrifuge (Huang, et al., 2024) and FE for  $\hat{z} = 3$  and  $\hat{z} = 6$  (with disturbance).

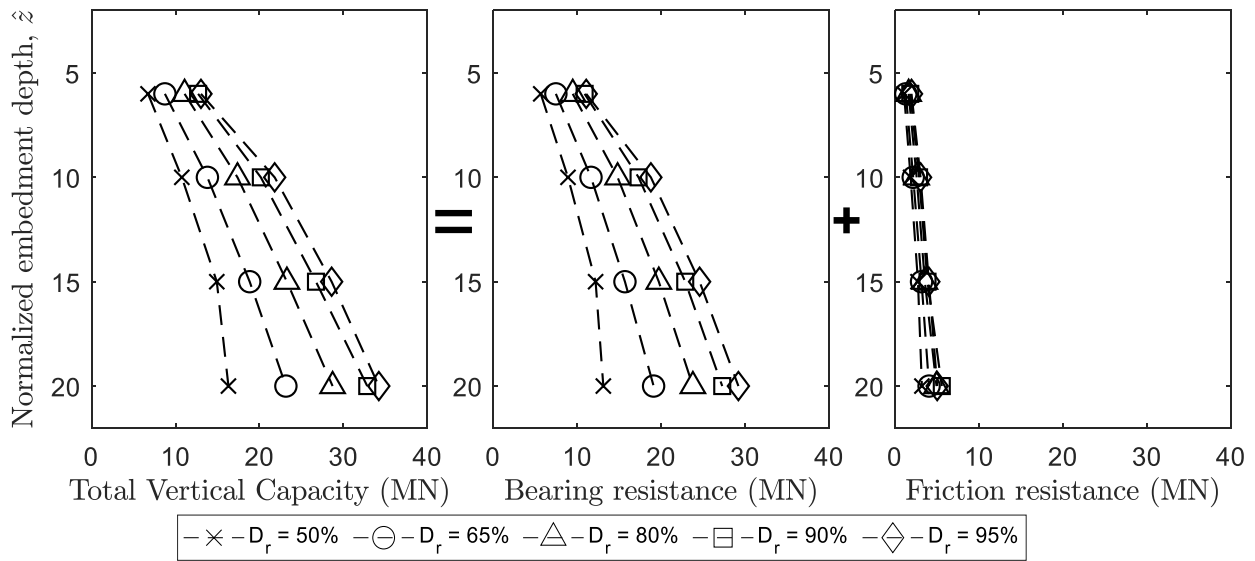


Figure 4. FEA predictions for total vertical capacity profile of DERA at different soil relative densities

Figure 5 presents the corresponding displacement contours which demonstrate the different failure mechanisms of DERA under the studied loading. A surface failure was observed in case of shallow embedments, which transitioned to localized flow around failure with an increase in the anchor embedment depths. The vertical bearing factors,  $N_q$  (defined as predicted bearing capacity upon the effective area (Gogoi R. , et al., 2023)) in Figure 6, further highlight this transition, where the  $N_q$  values increase with embedment till the transition depth, and then begin to decrease. The decrease in  $N_q$  with depth for the deeper embedments can be attributed to the implementation of a stress dependent soil profile (Bolton M. , 1986). The distinctive anchor responses predicted provided a means to quantify the point at which free-surface effects end. A ratio termed as the critical displacement ratio,  $\delta_{crit}$ , was introduced, defined in terms of the displacement predicted at the top of the domain (seabed level),  $(u_v)_{surface}$ , relative to the maximum displacement

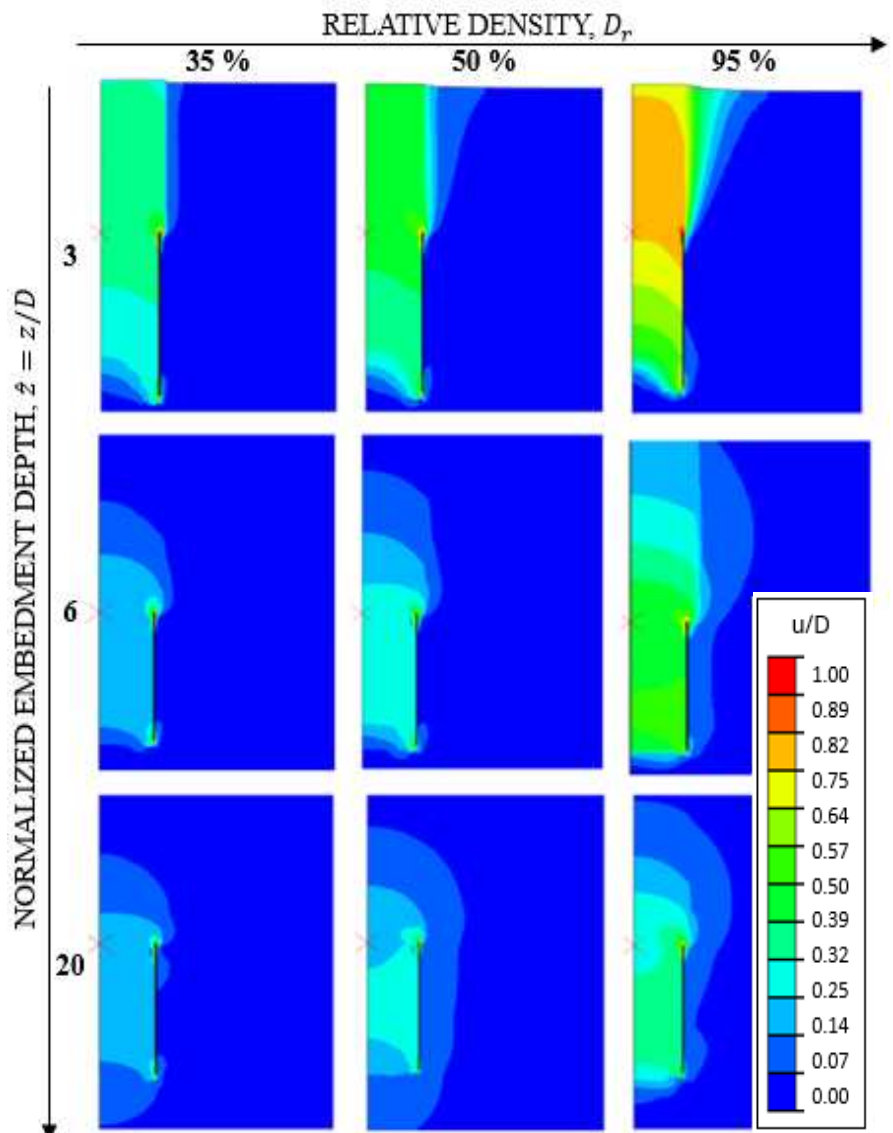


Figure 5. Displacement contours at failure.

predicted (at the top of the anchor),  $(u_v)_{max}$ :

$$\delta_{crit} = \frac{(u_v)_{surface}}{(u_v)_{max}} \quad (4)$$

For a reference relative density of 80%, a limit of 0.24 was estimated from the results of the numerical simulation, such that:

$$\delta_{crit} = \begin{cases} \geq 0.24; & \text{surface failure} \\ < 0.24; & \text{local flow around failure} \end{cases}$$

with  $\hat{z} (z/D) \geq 4.5$  for  $\hat{L}(L/D) = 1.5$  demonstrating a surface failure. Since DERA is most effective for deep embedments, subsequent investigations will be limited to the preferred localized flow around failure cases.

#### 4 EFFECT OF RELATIVE DENSITY

Figure 4 also shows the FE capacity predictions for the anchor under different initial state relative densities of the soil, where an increase in the vertical capacity with an increase in the soil density is observed, as expected. The corresponding displacement contours of the anchor at the defined failure threshold, presented in Figure 5, highlight the extent of soil mobilization within the ring of the anchor, resulting in the creation of a partial soil plug. Although plugging, especially in loose soils, is intuitively unlikely, the finite element simulations suggest that at least partial plugging occurs. The numerical simulations were studied by decomposing the vertical capacity into its contributing frictional and end bearing components as a function of the anchor wall thickness, which repeatedly reinforced the initial observation of the partial formation of a soil plug, where only a minor variation in the total capacity was observed, contrary to the theoretical expectation of a proportional change with the annular area, and with the degree of its formation reducing with depth and increasing with relative density. At a reference  $\hat{z}=6$ , a maximum soil plug displacement of 0.15 and 0.5 times the maximum anchor displacements was predicted for the lowest and highest simulated relative densities, respectively.

#### 5 CALCULATION FRAMEWORK

The findings and observation from the parametric test series provided the basis for the development of a framework to estimate the ultimate vertical capacity of DERA in drained sand, formulated as a function of the relative density of the soil and the embedment depth of the anchor (Figures 4 and 6). The model also exhibited

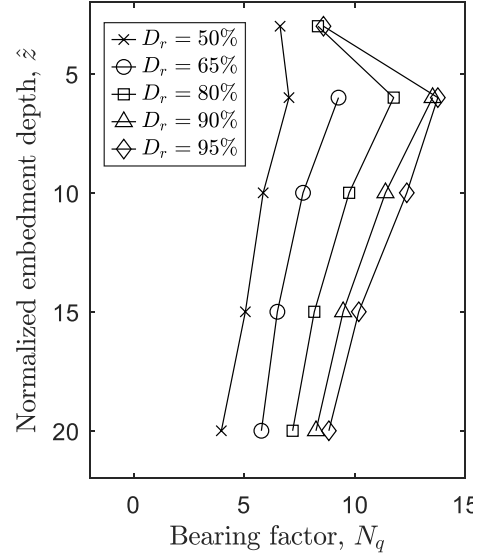


Figure 6. Vertical bearing factors for varying relative densities.

a second degree of dependency on the soil strength parameters, due to the adoption of a density and stress dependent soil profile in the FE model. The evaluation focused on normalized embedment depth  $\hat{z} \geq 6$ , and an anchor with 2.8 m diameter,  $D$ , aspect ratio,  $\hat{L}$  of 1.5 and wall thickness,  $t$  of  $D/160$ . Following established theoretical principles, the anchor capacity,  $Q_v$ , was expressed as a sum of a friction component ( $Q_f$ ) and tip bearing component ( $Q_t$ ) as follows:

$$Q_v = Q_f + Q_t = f_{s,av} A_{wall} + N_q (\sigma'_{v,tip} A_{top}) \quad (5)$$

where,  $f_{s,av} = 0.5K\sigma'_{v,wall} \tan \delta$  (Andersen et al. 2008) is the the average friction along the length of the anchor, and  $A_{wall}$  the effective area of only the outer wall;  $K$ =ratio between horizontal and initial vertical effective stress,  $\sigma'_{v,wall}$ =effective vertical stress, and  $\delta$ =internal friction angle. For the tip bearing component, the vertical bearing factor,  $N_q$ , is expressed as follows:

$$N_q = a(\hat{z})^b \quad (6)$$

where,  $\hat{z}$  is the normalized embedment depth ( $= z/D$ ), and  $a$  and  $b$  are coefficients empirically calibrated from the results of the parametric studies as second order polynomial functions of relative density,  $D_r$ :

$$a = -19.36 D_r^2 + 53.34 D_r - 5.59 \quad (7)$$

$$b = 0.26 D_r^2 - 0.19 D_r - 0.42 \quad (8)$$

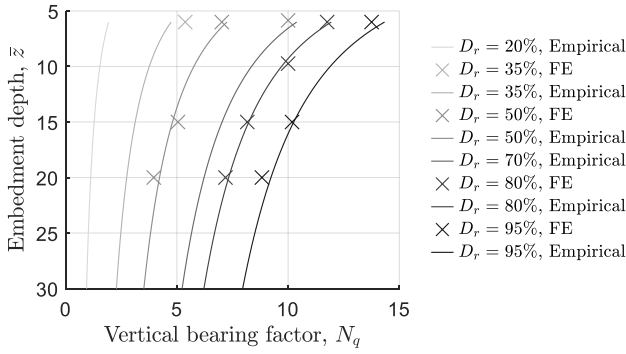


Figure 7. Bearing factors from empirical model vs FEA.

and,  $A_{top}$  is the gross cross-sectional area of the top face of the anchor, and  $\sigma'_{v.tip}$  the effective vertical soil stress level at its top. (Equations 7 and 8, requires  $D_r$  to be expressed as a decimal). While the normalization is in terms of total area, the various degrees of partial plugging and the weight of the soil plug are implicitly included in the bearing factor  $N_q$ . Figure 7 presents the back-calculated  $N_q$  values from the calibrated FE predictions ('X') for different initial soil densities, along with the corresponding predictions from the introduced model (solid lines), and Table 1 provides the subsequent total vertical capacities. The introduced calculation framework compared well with the predictions of the calibrated numerical model and thus can be proposed as a means to determine the ultimate vertical capacity of DERA in drained sand for design purposes.

Table 1. Total vertical capacity for DERA at  $\hat{z}=20$ .

| $D_r$<br>(%) | Calculated<br>(MN) | FE<br>(MN) | Difference<br>(%) |
|--------------|--------------------|------------|-------------------|
| 50           | 16.9               | 16.3       | 3.7               |
| 80           | 27.4               | 28.7       | 4.7               |
| 95           | 33.7               | 34.2       | 1.6               |

## 6 ANCHOR COMPARISON

Previous studies have demonstrated the theoretical effectiveness of DERA compared to conventional offshore anchors (Diaz, et al., 2016), either through cost analysis (Lee, Khan, Bello, & Aubeny, 2020) or in terms of its capacity in clay (Lee & Aubeny, 2021). The present study shifts the focus to evaluating DERA's vertical capacity in sand, highlighting its favorable anchor efficiency, defined as the ratio of the ultimate capacity to total weight (Aubeny C., 2017). The performance of DERA is compared against that of a well-established anchor system, the suction bucket, in dense sand ( $D_r = 80\%$ ) (Houlsby, Kelly, & Byrne, 2005). The results, presented in Figure 8, demonstrate the high efficiency of DERA, showcasing its key

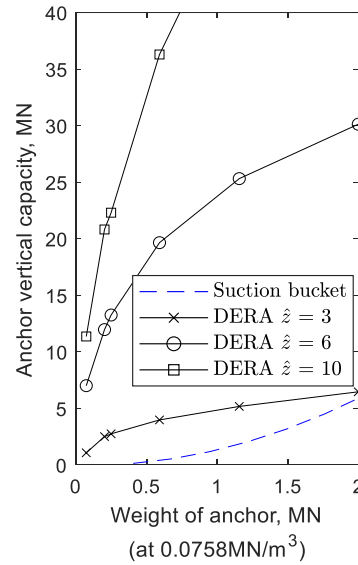


Figure 8. DERA vs. Suction bucket under vertical loading.

advantage of achieving significantly larger capacities at relatively low anchor weights due to deeper embedment depths. In contrast, the suction bucket requires continuous skirt length from the soil surface to achieve comparable results. The favorable results along with DERA's ability to meet the anchor load demands of a 15 MW turbine in the Celtic Sea (70 m) (Pillai, et al., 2022) as demonstrated in (Gogoi R., et al., 2023), strengthens the case for DERA as an effective solution for floating offshore wind farms in sand.

## 7 CONCLUSIONS

This study presents a framework for estimating the vertical capacity of the DERA in sand, as a function of key parameters such as embedment depth and relative soil density. The research offers insights into the anchor's failure mechanisms under vertical monotonic loads, demonstrating the transition from surface failure at shallow depths to localized flow-around failure at deeper embedment. These findings enhance the understanding of DERA's behavior in sands and provide a basis for optimizing its design and performance for offshore renewable energy applications.

## AUTHOR CONTRIBUTION STATEMENT

**R. Gogoi:** Writing - Original draft, Formal Analysis, Investigation, Methodology. **A. Aldawwas.:** Writing- Reviewing and Editing, Investigation, Methodology. **C. Aubeny:** Writing- Reviewing and Editing, Conceptualization, Funding acquisition, Methodology, Supervision. **D. Degroot:** Writing-

Reviewing and Editing, Conceptualization, Funding acquisition. **S. Arwade:** Writing- Reviewing and Editing, Conceptualization, Funding acquisition. **A. Martinez:** Writing- Reviewing and Editing, Conceptualization, Funding acquisition. **R. Beemer:** Writing- Reviewing and Editing, Conceptualization, Funding acquisition.

## ACKNOWLEDGEMENTS

The authors would like to acknowledge the support from National Science Foundation, award number CMMI-1936901 and CMMI-1936939 and the Texas A&M High Performance Research Computing facility for the use of their resources in running the numerous finite element analyses supporting this study.

## REFERENCES

- Al Hakeem, N. M. (2019). *Finite element investigation into the performance of embedded plate Anchors in Sand*. Doctoral Dissertation. Texas A&M University.
- AlHakeem, N., & Aubeny, C. (2019). Numerical Investigation of Uplift Behavior of Circular Plate Anchors in Uniform Sand. *Journal of geotechnical and Geoenvironmental Engineering*, 145(9), [https://doi.org/10.1061/\(ASCE\)GT.1943-5606.0002083](https://doi.org/10.1061/(ASCE)GT.1943-5606.0002083).
- Aldawwas, A. (2022). *Ultimate Load Capacity of Caisson Foundations and Anchors in Sand*. Doctoral dissertation. Texas A&M University.
- Andersen, K. H., Jostad, H. P., & Dyvik, R. (2008). Penetration Resistance of Offshore Skirted Foundations and Anchors in Dense Sand. *Journal of Geotechnical and Geoenvironmental Engineering*, 134(1)
- Aubeny, C. (2017). *Geomechanics of marine anchors*. CRC Press. <https://doi.org/10.4324/9781351237376>
- Aubeny, C. P., Diaz, B. D., Arwade, S. R., Degroot, D. J., Landon, M. E., Fontana, C., & Hollowell, S. T. (2019). *USA. US 2020/0407021 A1*.
- Aubeny, C., & Lee, J. (2021). Horizontal load capacity of Multiline ring anchor in soft clay. In: *International Symposium on Frontiers in Offshore Geotechnics*. Austin.
- Bastidas, A. M. (2016). *Ottawa F-65 Sand Characterization*. Doctoral Dissertation. University of California, Davis.
- Bolton, M. (1986). Strength and dilatancy of sands. *Geotechnique*, 36(1). <https://doi.org/10.1680/geot.1986.36.1.65>
- Diaz, B., Rasulo, M., Aubeny, C., Fontana, C., Arwade, S., DeGroot, D., & Landon, M. (2016). Multiline anchors for floating offshore wind towers. In: *Oceans*, Monterey, USA
- Fontana, C., Hallowell, S., Arwade, S., DeGroot, D., Landon, M., Aubeny, C., . . . Ozmutlu, S. (2018). Multiline anchor force dynamics in floating offshore wind turbines, *Wind Energy*, 21(11), 1177-1190, <https://doi.org/10.1002/we.2222>.
- Gogoi, R. (2024). *A numerical study on the multiline ring anchor in sand*, Doctoral Dissertation, Texas A&M University.
- Gogoi, R., Aldawwas, A., Aubeny, C., Martinez, A., Huang, L., DeGroot, D., . . . Beemer, R. (2023). Numerical analyses of a multiline ring anchor for floating offshore wind turbines in sand, In: *10th European Conference on Numerical Methods in Geotechnical Engineering*, London, UK. <https://doi.org/10.53243/NUMGE2023-336>
- Gogoi, R., Aubeny, C., Watson, P., & Bransby, F. (2021). Uplift capacity of suction caissons in sand for general conditions of drainage. In: *Offshore Mechanics and Arctic Engineering*, Online, <https://doi.org/10.1115/OMAE2021-61663>
- Houlsby, G., Kelly, R., & Byrne, B. (2005). The tensile capacity of suction caissons in sand under rapid loading. In: *1st International Symposium on Frontiers in Offshore Geotechnics*, 10.1201/NOE0415390637.ch40
- Huang, L., Martinez, A., Aubeny, C., DeGroot, D., Arwade, S., & Beemer, R. (2025). Centrifuge modelling of the monotonic capacity of offshore ring anchors in sand. In: *Geotechnical Frontiers* <https://doi.org/10.1061/9780784486009.030>
- Lee, J., & Aubeny, C. (2021). Lateral Undrained Capacity of a Multiline Ring Anchor in Clay. *International Journal of Geomechanics*, 21(5), [https://doi.org/10.1061/\(ASCE\)GM.1943-5622.0001995](https://doi.org/10.1061/(ASCE)GM.1943-5622.0001995)
- Lee, J., Khan, M., Bello, L., & Aubeny, C. (2020). Cost Analysis of Multiline Ring Anchor System for Offshore Wind Farm. *45th Annual Conference on Deep Foundations*, (p.p. 484-493).
- Pillai, A., Gordelier, T., Thies, P., Dormenval, C., Wray, B., Parkinson, R., & Johanning, L. (2022). Anchor loads for shallow water mooring of a 15 MW floating wind turbine. *Ocean Engineering*, <https://doi.org/10.1016/j.oceaneng.2022.111816>
- Vesic, A. (1977). *Design of pile foundations*. Synthesis of Highway Practice 42, Transportation Research Board.
- Vesic, A. S. (1972). Expansion of cavities in infinite soil mass. *Journal of Soil Mechanics & Foundations Div*, 98, 265-290.

# INTERNATIONAL SOCIETY FOR SOIL MECHANICS AND GEOTECHNICAL ENGINEERING



*This paper was downloaded from the Online Library of the International Society for Soil Mechanics and Geotechnical Engineering (ISSMGE). The library is available here:*

<https://www.issmge.org/publications/online-library>

*This is an open-access database that archives thousands of papers published under the Auspices of the ISSMGE and maintained by the Innovation and Development Committee of ISSMGE.*

*The paper was published in the proceedings of the 5th International Symposium on Frontiers in Offshore Geotechnics (ISFOG2025) and was edited by Christelle Abadie, Zheng Li, Matthieu Blanc and Luc Thorel. The conference was held from June 9<sup>th</sup> to June 13<sup>th</sup> 2025 in Nantes, France.*